TRANSPORT, CORRELATION AND STRUCTURAL DEFECTS

Edited by
Hellmut Fritzsche

World Scientific

Матеріал, захищений авторським правом

Advances in Disordered Semiconductors — Vol. 3

TRANSPORT, CORRELATION AND STRUCTURAL DEFECTS

Transport, Correlation and Structural Defects Downloaded from www.worldscientific.com
by 77.122.155.157 on 02/07/17. For personal use only.

Transport, Correlation and Structural Defects Downloaded from www.worldscientific.com
by 77.122.155.157 on 02/07/17. For personal use only.

ADVANCES IN DISORDERED SEMICONDUCTORS

Editor-in-charge: Hellmut Fritzsche

Published:

Volume 1 Amorphous Silicon and Related Materials
edited by Hellmut Fritzsche

Volume 2 Hopping and Related Phenomena
edited by Hellmut Fritzsche and Michael Pollak

Transport, Correlation and Structural Defects Downloaded from www.worldscientific.com
by 77.122.155.157 on 02/07/17. For personal use only.

Advances in Disordered Semiconductors — Vol. 3

TRANSPORT, CORRELATION AND STRUCTURAL DEFECTS

Edited by
Hellmut Fritzsche
The James Franck Institute
The University of Chicago
Chicago, USA

World Scientific
Singapore • New Jersey • London • Hong Kong

Transport, Correlation and Structural Defects Downloaded from www.worldscientific.com
by 77.122.155.157 on 02/07/17. For personal use only.

Published by

World Scientific Publishing Co. Pte. Ltd.
P O Box 128, Farrer Road, Singapore 9128
USA office: 687 Hartwell Street, Teaneck, NJ 07666
UK office: 73 Lynton Mead, Totteridge, London N20 8DH

Library of Congress Cataloging-in-Publication data is available.

TRANSPORT, CORRELATION AND STRUCTURAL DEFECTS

Copyright © 1990 by World Scientific Publishing Co. Pte. Ltd.

All rights reserved. This book, or parts thereof, may not be reproduced in any form or by any means, electronic or mechanical, including photocopying, recording or any information storage and retrieval system now known or to be invented, without written permission from the Publisher.

ISBN 9971-50-973-3

Printed in Singapore by Utopia Press.

PREFACE

This series presents new ideas and recent developments in our understanding of disordered semiconductors. This field covers many material systems and attracts scientists of very different specializations. It is therefore important that the articles in this series contain sufficient background material so that they communicate across barriers of specialization and are accessible to graduate students. An important goal of Advances in Disordered Semiconductors is to present interesting as well as controversial subjects at a fast publication schedule. Some of the same topics are addressed by different authors in order to illuminate problems from different angles and to highlight unresolved questions.

Hellmut Fritzsche
October 15, 1990

Transport, Correlation and Structural Defects Downloaded from www.worldscientific.com
by 77.122.155.157 on 02/07/17. For personal use only.

This page is intentionally left blank

Transport, Correlation and Structural Defects Downloaded from www.worldscientific.com
by 77.122.155.157 on 02/07/17. For personal use only.

INTRODUCTION

Disordered materials offer new and unexpected insights into the structure of solids and the ways charge carriers move and interact with their environment. Regardless of whether the atomic arrangement has translational symmetry or not, the nearest neighbor coordination in covalent semiconductors is determined by the chemical valency of the atoms. Moreover, in both crystalline and noncrystalline semiconductors, electronically active defects are associated with those few atoms that happen to be over - or under coordinated. These defects include donor and acceptor dopants as well as native coordination defects.

Despite these similarities in chemical origin, these defects can undergo bonding rearrangements much more readily in noncrystalline than in crystalline semiconductors. The reason for this may be related to at least two factors. For one, the lack of periodicity allows for larger topological freedom and thus for a wider spectrum of bond energies including weak and strained bonds that are more accessible to changes. A second reason is the greater degree of localization of electrons and holes in disordered potentials. When this localization approaches covalent bond dimensions one expects a strong interplay between carrier occupancy of such localized states and the local bonding environment which produces these states.

Given sufficient time and thermal excitation this interaction comes to a thermodynamic equilibrium state in which the number of active dopants and defects depend only on temperature. At lower temperatures, a nonequilibrium change in carrier occupancy will cause changes in bond coordinations and thus in the number of active defects which persist for long times. Studies of such carrier-induced metastable structural changes in non-crystalline semiconductors have led to an awareness of their presence in crystals particularly at their surfaces and interfaces.

Charge transport is of course strongly affected by the localization of carriers in disordered potentials. Early work focused on hopping conduction in doped crystalline semiconductors at low temperatures where conduction in extended states is frozen out. In amorphous semiconductors the quasi-continuous distribution of localized states in the pseudogap sets new and interesting conditions for electronic transport and recombination of photo-excited carriers. Polymers, oxide glasses, boron and boron-rich compounds as well

Transport, Correlation and Structural Defects Downloaded from www.worldscientific.com
by 77.122.155.157 on 02/07/17. For personal use only.

as mesoscopic systems are other examples in which electronic processes are governed by localization effects.

The first part of this volume presents new results and ideas on the subjects dealing with the local bonding structure in amorphous and vitreous semiconductors. These include the local bonding structure in chalcogenide glasses containing metal atoms, the interaction of local vibrational modes with their local bonding environment, and new models for the H-bonding configurations and complexes in hydrogenated amorphous silicon that are associated with the metastable changes in defect and dopant concentrations.

The second part is devoted to questions of low temperature hopping transport and recombination of photocarriers in disordered semiconductors as a function of frequency and at high electric fields. One chapter is devoted to anomalous behavior of low temperature hopping conduction in p-type GaSb which appears at relatively high fields and uniaxial stresses. The last chapter discusses new aspects of transport in relaxation case semiconductors whose dielectric relaxation time is long compared to the carrier lifetime.

Transport, Correlation and Structural Defects Downloaded from www.worldscientific.com
by 77.122.155.157 on 02/07/17. For personal use only.

CONTENTS

Preface v

Introduction vii

Chapter 1: STRUCTURE AND DEFECTS

A General Structural Model for Amorphous Semiconductors
P.C. Taylor, Z.M. Saleh and Jeffrey Z. Liu 3

Persistent Infrared Spectral Hole Burning of Impurity Vibrational Modes in Chalcogenide Glasses
S. P. Love and A.J. Sievers 27

Hydrogen Complexes in Amorphous Silicon
W.B. Jackson and S.B. Zhang 63

Thermally Induced Metastable Processes in Amorphous Hydrogenated Silicon. Fluctuon Model of a-Si:H
S.B. Aldabergenova, N.A. Feoktistov, V.G. Karpov, K.V. Koughia, A.B. Pevtsov and V.N. Solovijev 129

Chapter 2: TRANSPORT AND RECOMBINATION

Hopping Photoconductivity in Amorphous Semiconductors: Dependence on Temperature, Electric Field and Frequency
B.I. Shklovskii, E.I. Levin, H. Fritzsche and S.D. Baranovskii 161

Optically Excited Localized Electrons and Photoconductivity of Disordered Semiconductors
I. P. Zvyagin 193

Transport, Correlation and Structural Defects Downloaded from www.worldscientific.com by 77.122.155.157 on 02/07/17. For personal use only.

Tunnel Recombination in 4-Fold Coordinated Disordered Semiconductors
K.V. Koughia and I.S. Shlimak 213

Anomalous Hopping Transport in p-GaSb
David Aladashvili, Z.A. Adamiya, K.G. Lavdovskii and H. Fritzsche 253

Transport Phenomena in Relaxation Case Inhomogeneous Semiconductors
Yu. P. Drozhov 271

Subject Index 301

Author Index 305

Transport, Correlation and Structural Defects Downloaded from www.worldscientific.com
by 77.122.155.157 on 02/07/17. For personal use only.

TRANSPORT, CORRELATION AND STRUCTURAL DEFECTS (pp. 129 – 158)
edited by Hellmut Fritzsche

© 1990 World Scientific Publishing Company

THERMALLY INDUCED METASTABLE PROCESSES IN AMORPHOUS HYDROGENATED SILICON. FLUCTUON MODEL OF a–Si:H

S.B. Aldabergenova, N.A. Feoktistov, V.G. Karpov, K.V. Koughia, A.B. Pevtsov and V.N. Solovijev**

A.F. Ioffe Physico-Technical Institute,
Leningrad 194021, USSR

*M.I. Kalinin Politechnical Institute,
Leningrad 195251, USSR

1. INTRODUCTION

Recently Street et al.[1–5] have shown that the electronic properties of doped hydrogenated amorphous silicon (*a*–Si:H) are strongly influenced by hydrogen diffusion, stimulated by thermal treatment. The interpretation of their experimental observations is mainly based on assumptions about the doping mechanism in *a*–Si:H proposed earlier by Street.[6] At the same time similar effects were found in undoped *a*–Si:H samples.[7–11] If the nature of these phenomena are similar in doped and undoped *a*–Si:H their strong dependence on doping should not be essential. In the following we discuss some other aspects of the interpretation,[1–4] that seem not be convincing. We thus suppose that the effect of hydrogen diffusion on the electronic properties of *a*–Si:H needs further investigation.

In this paper we discuss some new experimental results regarding the changes in the electronic properties of undoped *a*–Si:H under different conditions of thermal annealing and cooling which govern hydrogen diffusion. The following interpretation consists of two parts: the first is a phenomenological model and the second is its microscopic concretization. The proposed phenomenological model is free from assumptions about the detailed mechanism of the interaction between electrons and the hydrogen subsystem.

Another part deals with a detailed but rather general model of the interaction mechanism between electrons and hydrogen atoms. This model is based on recent proposals by Karpov and Solovijev[12] about fluctuonic states in amorphous semiconductors. We discuss this model in detail while comparing it with the experimental results.

Матеріал, захищений авторським правом

2. REVIEW OF PREVIOUS EQUILIBRATION MODEL

Before considering new results let us review some details of the interpretation given in references 1-4. Fig. 1a shows typical dependences of the conductivity on temperature from these papers.[1,2] The main feature of these curves is the change in activation energy at a certain characteristic equilibrium temperature T_E. The explanation of this fact is based on two suppositions. The first is a very specific dependence of the density of localized states as a function of energy, $g(\varepsilon)$, in the mobility gap (Fig. 1b). The second is the doping mechanism which assumes that electron trapping in deep states is accompanied by defect creation. The expected abrupt decrease of the density of states $g(\varepsilon) \propto \exp(-\varepsilon/\varepsilon_o)$ with the characteristic energy $\varepsilon_o < kT_E$ plays an important role. This decrease takes place at the energy $\varepsilon > \varepsilon_1$ and at $\varepsilon < \varepsilon_1$ the distribution $g(\varepsilon)$ is supposed to be rather smooth. These assumptions yield a peak in the thermal carrier distribution at an energy $\varepsilon \approx \varepsilon_1$ above the Fermi-level μ at $T > T_E$. After sufficiently fast cooling to $T < T_E$ the electrons remain at $\varepsilon \approx \varepsilon_1$ for a long time because defects which are needed for their thermal

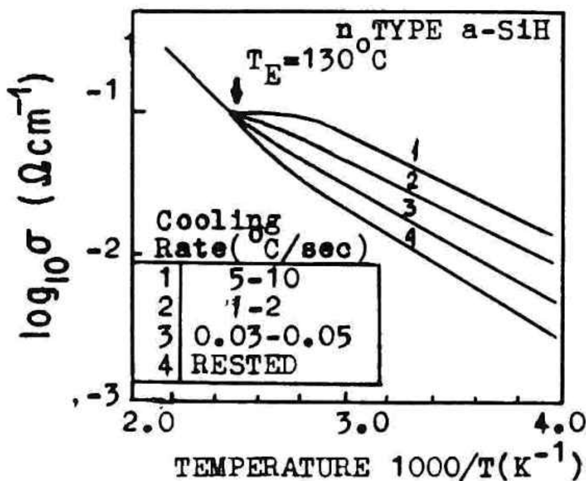

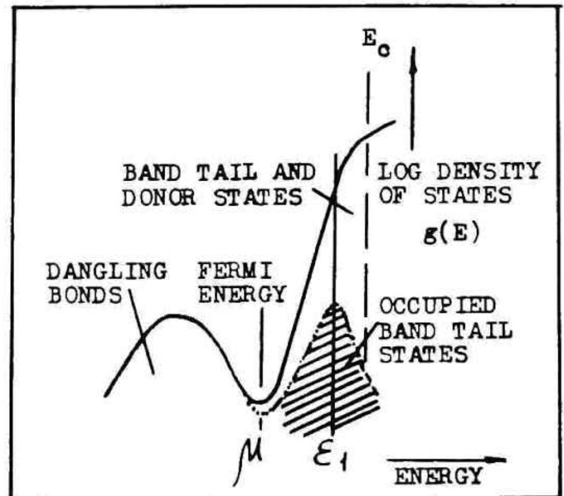

Fig.1a Temperature dependence of the conductivity of n-type a-Si:H measured after different thermal treatments: 1-3 cooling at different rates immediately after annealing at high T: 4 - the sample has been kept at room temperature for two months. (From Street et al., ref. 1).

Fig.1b Schematical diagram of localized density of states distribution in n-type a-Si:H. Shaded region is electron density in conduction band tail at elevated temperature. (After ref. 1).

Матеріал, захищений авторським правом

relaxation are late to create. As a consequence, the conductivity activation energy after rapid cooling drops from the value μ to a value $\varepsilon_1<\mu$ (see Fig 1b) in accordance with the experimental data (Fig. 1a).

It should be emphasized that the above explanation depends sensitively on the details of the model and its parameters. For example, the condition $\varepsilon_o<kT_E$ at $T_E\approx100^oC$ can be fulfilled for a conduction band tail for which $\varepsilon_o/k\approx300$K.[13] But for the valence band tail the value $\varepsilon_o/k\approx500$K.[13] is significantly greater than T_E. This means that the above interpretation seems not to be valid for explaining the behavior of p-type samples in contrast with the observation that the experimental results are qualitatively the same in n-type and p-type a−Si:H. Moreover, temperature dependences of the conductivity similar to those of n-type material[1] were observed also in undoped samples.[7,8]

Another point of Street et al.'s explanation[1–4] concerns the kinetics of the persistent conductivity after fast cooling. In reference 1 this kinetics was approximated by

$$n_{BT}\propto t^{-\gamma}, \tag{1}$$

where n_{BT} is the electron concentration in the conduction band tail and γ~0.1. But in subsequent papers[2–4] Street et al. proposed the following more complicated relations commonly used in glasses:

$$n_{BT}\propto\exp\{-(\frac{t}{\tau})^{\beta}\},\quad \tau=\tau_o\exp(\frac{E_\tau}{kT}). \tag{2}$$

These authors[2–4] suggest a theoretical explanation of Eq. (2) on the basis of two suppositions. The first is that slow relaxation is caused by a rearrangement of the atomic system, for example, by defect creation, which occurs with hydrogen participation and is limited by the hydrogen diffusion rate. The second is that the diffusion coefficient D is a function of time

$$D\propto t^{\alpha}\exp(-\frac{E_D}{kT}), \tag{3}$$

where E_D is the activation energy of diffusion. Eq. (2) was independently deduced by substituting Eq. (3) into the kinetic relation

Матеріал, захищений авторським правом

$$\frac{dn_{BT}}{dt} \propto -Dn_{BT} \tag{4}$$

which leads to Eq. (2) with

$$\beta = 1-\alpha \text{ and } E_\tau = E_D/\beta \tag{5}$$

We note two inconsistencies. The first is that the relation (5) between E_τ and E_D contradicts earlier experimental results,[1] where $E_\tau < E_D$ and $\beta < 1$ (for example, $E_D \approx 1.2$ eV, $E_\tau \approx 0.95$ eV, and $\beta = 0.7$). The second is that according to references 1 and 2 Eq. (3) implies dispersive diffusion of hydrogen. As a consequence the profile of the hydrogen distribution should become non-gaussian with diffusion. On the contrary the results of reference 14 show that diffusion leads to the common diffusion profile that is described by an error function. The latter observation disagrees with Eq. (3).

[Comment by editor: the last statement of the authors is incorrect. J. Kakalios and W.B. Jackson have shown that dispersive hydrogen diffusion still results in an error function profile of the hydrogen concentration. See p. 231 in "Amorphous Silicon and Related Materials" ed. H. Fritzsche (World Scientific, Singapore, 1988)].

3. EXPERIMENTAL RESULTS

Our investigations were carried out on undoped a-Si:H samples, prepared by radio frequency glow discharge decomposition of 100% silane. Quartz was used as a substrate and the films were 0.5-1 μm thick. The deposition temperature was varied between 200° and $270^o C$. The reactor was made of stainless steel and was pumped to 2×10^{-6} Torr before each deposition. The air leakage was $10^{-5}-10^{-6}$liters Torr/s. The flow rate of silane was chosen to be $0.1-1 cm^3/s$, and the pressure was 0.1-0.4 Torr. Aluminum contacts were deposited by magnetron sputtering.

The optical gap of our samples was $E_o = 1.65-1.7$ eV as obtained from a Tauc plot. The electrical and optical measurements were carried out in a special stainless steel chamber at a vacuum better than 5×10^{-4} Torr. The temperature was varied between 80 and 500K.

Amorphous silicon samples can show quite different temperature dependences of the conductivity $\sigma(T)$ depending on the deposition parameters such as pressure,

Матеріал, захищений авторським правом

gas flow rate, and r.f. power. These $\sigma(T)$ curves might have only one activation energy or alternatively might show several kinks. In the following we discuss the electrical and optical properties of samples which have two kinks in their $\sigma(T)$ dependencies. An example of such a $\sigma(T)$ dependence is shown in Fig. 2. The measurements were made while the sample was heated after a prolonged rest at room temperature. Three regions may be distinguished. In regions I and III the activation energies E_A=0.5 eV and E_A=0.65 eV are close to each other and practically do not depend on the heating rate. In region II the activation energy is E_A=1.1 eV, a value that is considerably larger than $E_o/2$.

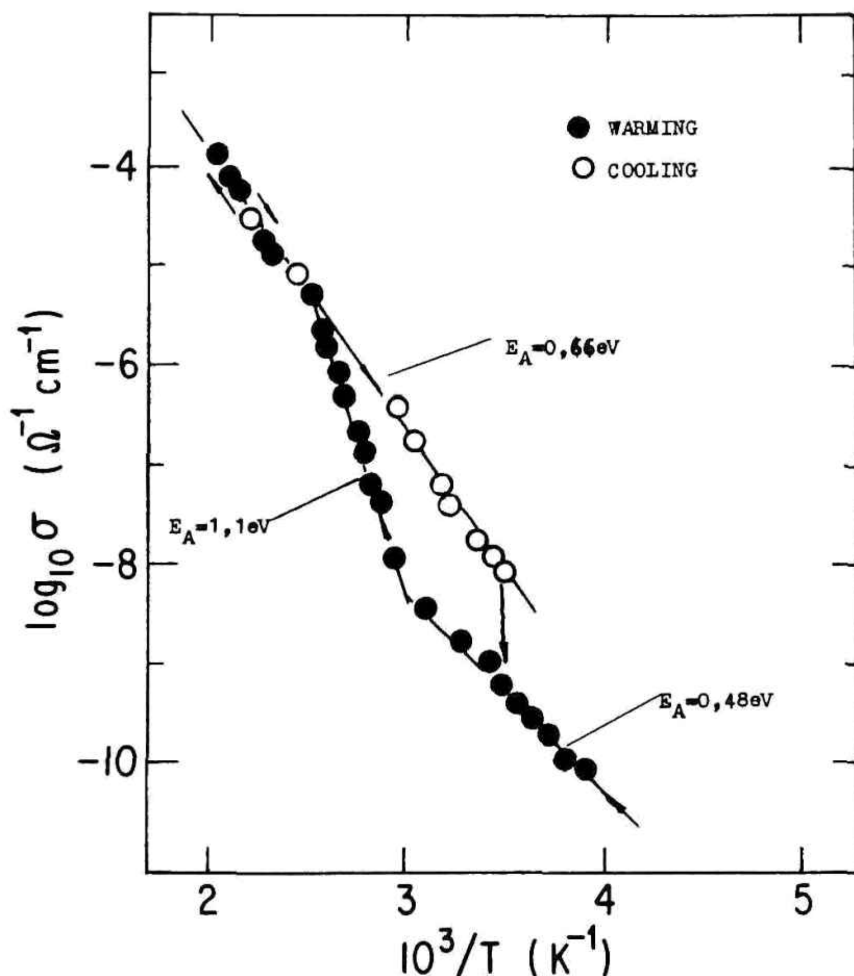

Fig.2 Temperature dependence of the conductivity during heating (black circles) and cooling (open circles). Vertical arrow is the conductivity relaxation at room temperature during 24 hours.

Матеріал, захищений авторським правом

In a series of samples the activation energies in regions I and III were in the 0.4 - 0.68 eV range while in region II it could reach values of about 1.5 - 1.7 eV in agreement with earlier results of Andreev et al.[7,8] Region II is observed between 0 and $100^o C$. The room temperature conductivities measured before heating and after cooling could differ by one order of magnitude. After cooling to room temperature the conductivity slowly relaxes to its initial value. The kinetics of this relaxation is shown in Fig. 3. It can be approximated by the power law $\sigma \propto t^{-\gamma}$ with

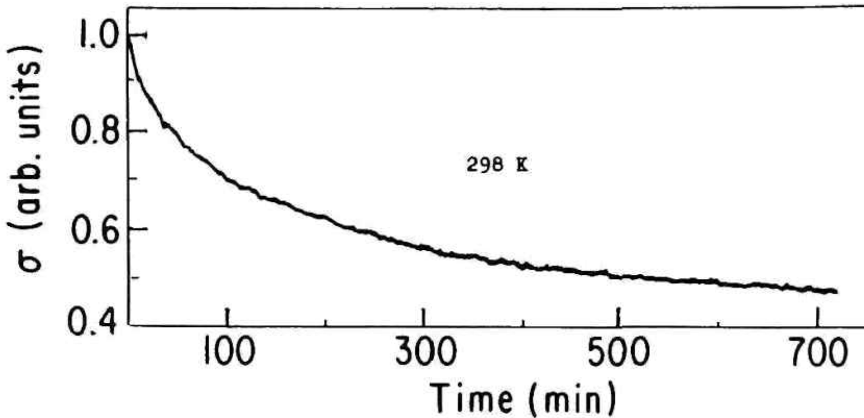

Fig.3 Conductivity relaxation at room temperature after cooling from $200^o C$ down to room temperature $\sigma \propto T^{-\gamma}$, $\gamma \approx 0.45$.

$\gamma \approx 0.45$. The power law of relaxation agrees with the results of Street et al.[1] Besides measuring $\sigma(T)$ we carried out the following experiments. The sample was annealed at $200^o C$ for 10 minutes and then rapidly cooled down to room temperature. It was then heated to $T_A < 200^o C$ where it was kept for 10 minutes. Then it was cooled to room temperature where the conductivity $\sigma_{\mathrm{room}}(T_A)$ was measured. The value of this conductivity turned out to depend on T_A. At the same time the experimental results did not show any dependence on the heating and cooling rates in the range $0.05^o C/s < dT/dt < 0.5^o C/s$; the fastest rate was limited by the design of our chamber. The above cyclic measurements were repeated for several T_A, in each case heating up to $200^o C$ was avoided in contrast to earlier studies.[1,2] The results are presented in Fig. 4. It should be noted that the non-monotonic behavior of $\sigma_{\mathrm{room}}(T_A)$ can be understood because the two extreme points refer to one preliminary annealing at $200^o C$, cooling down to room temperature and measuring $\sigma_{\mathrm{room}}(T_A = 200^o C)$. The information about the relevant physical processes is contained in the position of the peak in this curve and will be discussed in detail in the next section.

Матеріал, захищений авторським правом

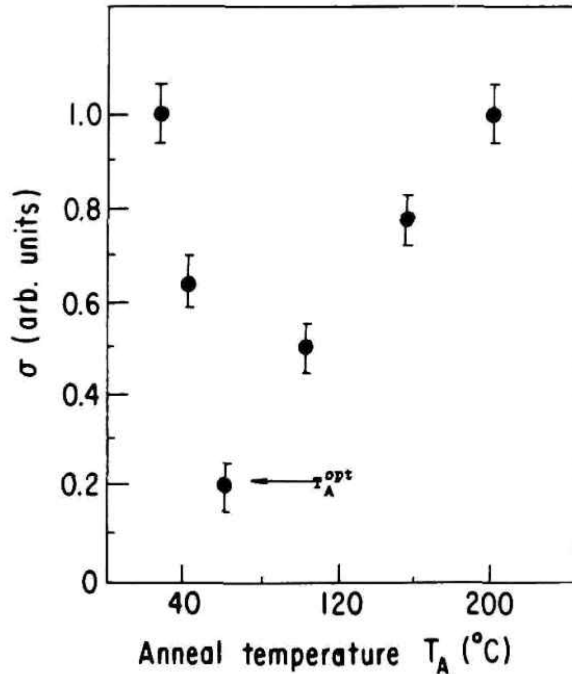

Fig.4 Room temperature conductivity as a function of annealing temperature T_A measured after temperature cycling as described in the text.

By anology with $\sigma(T_A)$ measurements, cyclic measurements of $\alpha(h\nu)$ in the $h\nu$=0.8–1.6 eV region were carried out. The spectral dependencies $\alpha(h\nu)$ in the region of low subbandgap absorption were measured by the constant photocurrent method.[15] The measurements were carried out with coplanar contacts. The absolute values of α were determined by normalizing the absorption values with direct transmission measurements in the high α regime. Fig. 5 shows an example of the $\alpha(h\nu)$ dependence measured at room temperature for a sample previously annealed at $200^o C$. Its shape correlates well with results of other authors.[15] The exponential Urbach slope $\alpha \propto \exp(h\nu/\varepsilon_o)$ in the 1.4 eV $< h\nu <$1.6 eV region and the subbandgap absorption shoulder at $h\nu \approx$1.0–1.2 eV are clearly seen. Figs. 6 and 7 show the Urbach parameter ε_o and the shoulder absorption $\alpha(h\nu$=1.2 eV) as a function of T_A, which were measured as described earlier. As in the case of the $\sigma(T_A)$ curve this procedure again yields a coincidence of the left and right extrema points of the $\varepsilon_o(T_A)$ and $\alpha_{1.2}(T_A)$ dependencies. It is worth noting that the extrema positions coincide for all three curves and are situated near $T_A \approx 60^o C$.

Матеріал, захищений авторським правом

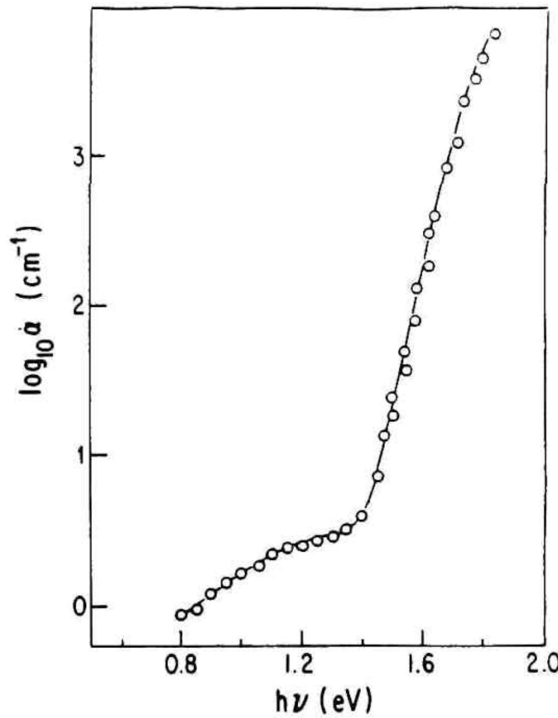

Fig.5 Spectral dependence of absorption coefficient of a–Si:H measured by the constant photocurrent method.

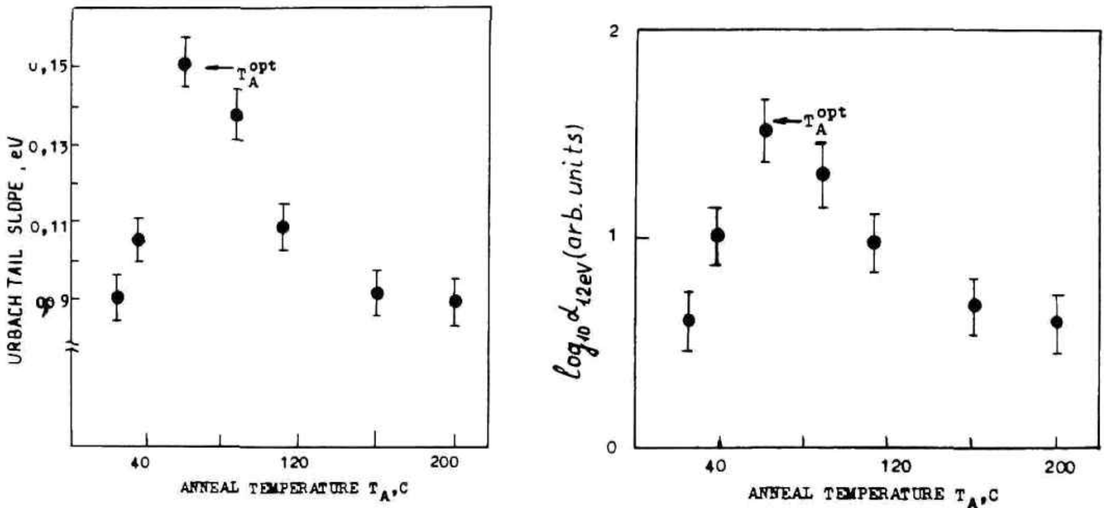

Fig.6 Urbach tail slope as a function of annealing temperature T_A measured after temperature cycling as described in text.

Fig.7 Absorption coefficient α at $h\nu$=1.2 eV as a function of annealing temperature T_A after temperature cycling as described in text.

Матеріал, захищений авторським правом

4. PHENOMENOLOGICAL INTERPRETATION

The longtime relaxations of the sample parameters after annealing and their sensitivity to annealing details suggest that these phenomena are related to a reconstruction of the atomic system. We do not try here to guess what kind of reconstruction occurs. From a phenomenological point of view each microscopic transition from one stable state to another produces a change ΔE in the energy of the system as a result of overcoming a potential barrier. Such a transition can be described by a double well potential as sketched in Fig. 8. In an amorphous system the parameters of the double well potential, such as the asymmetry ΔE and the barrier height V, will be randomly distributed. The simplest assumption is that these distributions are uniform in the ranges $0 \leq \Delta E \leq \Delta_o$ and $V_{min} \leq V \leq V_{max}$. This assumption is valid for explaining the two-level tunneling anomalies in the heat conductivity, specific heat and sound absorption at very low temperature in glasses.[16,17]

Double-well potential models were applied to a–Si:H earlier by Stutzmann[18] and Redfield.[19] We develop it here by considering possible variations of parameters caused by the disorder in amorphous systems. We assume that variations in physical parameters of a–Si:H observed in our experiments reflect variations in occupancies of potential wells. Let us analyze the results of the measurements presented in Figs. 4, 6 and 7 from this point of view. In this model the situation is an follows: (1) at the beginning the two-well potential is kept at the temperature T_A^i for a time, which is sufficiently long to establish thermodynamical equilibrium; (2) then the temperature falls to a lower value T_A^f so fast that the system becomes frozen in; (3) after a short time the temperature rises rapidly to a value $T_A > T_A^f$ and

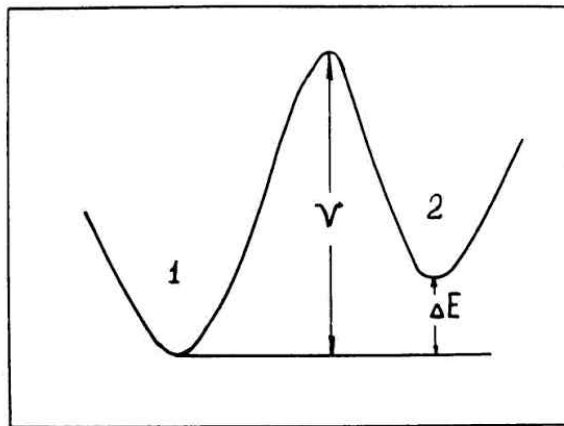

Fig.8 Double-well potential with barrier height V and asymmetry ΔE.

Матеріал, захищений авторським правом

is kept constant there for a time t; (4) the temperature drops to T_A^f where the measurements are carried out. In this scheme the changes in temperature can be regarded as instantaneous because we did not observe any dependence on the cooling and heating rates between 0.05 and 0.5 degrees/sec.

It is clear that the second step may be omitted for theoretical modelling. The temperature is assumed to jump directly from T_A^i to T_A. The fourth step too is not important because the temperature drop from T_A to T_A^f freezes the occupancies of the wells at values corresponding to the temperature T_A. We then have the following theoretical problem. In the initial state the two-well potential is in thermodynamical equilibrium at temperature T_A^i. The changes in well occupancies should be evaluated after a sharp decrease in temperature from T_A^i to T_A. First, the solution will be given for only one double well potential. It will then be averaged over a random distribution of potentials.

Let $P_\uparrow$ and $P_\downarrow$ be the transition probabilities from the lower to the upper minima and vice versa, and let m be the occupancy of the lower minimum. We then obtain the kinetic equation:

$$\frac{dm}{dt} = -mP_\uparrow + (1-m)P_\downarrow \tag{6}$$

with the initial condition

$$m = m_i \equiv m(t=0) = P_\downarrow(T_A^i)\tau(T_A^i) \tag{7}$$

The solution of (6) is

$$m = P_\downarrow(T_A^i)\tau(T_A^i)e^{-t/\tau} + P_\downarrow\tau(1-e^{-t/\tau}) \tag{8}$$

where the relaxation time

$$\tau = (P_\uparrow + P_\downarrow)^{-1} \tag{9}$$

is a function of T_A. It should be noted that $P_\uparrow/P_\downarrow = \exp(-\Delta E/kT)$, so the $P_\downarrow\tau$ product in Eq. (8) can be expressed as

$$P_\downarrow\tau = [1+\exp(-\frac{\Delta E}{kT_A})]^{-1} = \frac{1}{2} + \frac{1}{2}\tanh(\frac{\Delta E}{2kT_A}) \equiv \overline{m}(\Delta E, T_A) \tag{10}$$

with the average value

$$\overline{m}(T_A) \equiv \langle\overline{m}(\Delta E, T_A)\rangle = \frac{1}{2} + \frac{kT_A}{\Delta_o}\ln\cosh(\frac{\Delta_o}{2kT_A}) \tag{10a}$$

Матеріал, захищений авторським правом

The value $\overline{m}$ is the average occupancy of the lower well at T_A and does not depend on the barrier height between the two wells. So the occupancy change is

$$\Delta\overline{m} = [\overline{m}(\Delta E, T_A) - \overline{m}(\Delta E, T_A^i)](1 - e^{-t/\tau}) \qquad (11)$$

Eq. (11) predicts already a nonmonotonic dependence of $\Delta\overline{m}$ on T_A that is very similar to those shown in Figs. 4, 6 and 7. The qualitative explanation is quite clear. At low T_A the relaxation time τ is much greater than any possible time of measurements, i.e., $\tau \gg t$ so $\Delta\overline{m} \to 0$ according to Eq. (11). This case corresponds to the left extremal points of the dependencies shown in Figs. 4, 6 and 7. At high T_A, that is at $T_A \to T_A^i$, $\Delta\overline{m} \to 0$, too, because $\overline{m}(\Delta E, T_A) \to \overline{m}(\Delta E, T_A^i)$ according to Eq. (11). This case seems to correspond to the right extremal points of the dependencies shown in Figs. 4, 6 and 7.

To advance comparison with experimental data, Δm should be averaged over the distribution of two-well potentials:

$$<\Delta m> \approx \int_0^{\Delta_o} \frac{d\Delta E}{\Delta_o} \int_{\tau_{min}}^{\tau_{max}} \frac{d\tau}{\tau} (ln\frac{\tau_{max}}{\tau_{min}})^{-1} \Delta\overline{m}(\Delta E, \tau) \qquad (12)$$

where

$$\tau_{max} = \tau_o \exp(V_{max}/kT_A), \quad \text{and } \tau_{min} = t_o \exp(V_{min}/kT_A). \qquad (13)$$

In Eq. (12) we took into account that a uniform barrier height distribution leads to a time relaxation distribution proportional to τ^{-1}. Integration in Eq. (12) yields

$$<\Delta m> = \frac{k^2 L}{\Delta_o \delta V}(T_A - T_t)[T_A^i \ln\cosh(\frac{\Delta_o}{2kT_A^i}) - T_A \ln\cosh(\frac{\Delta_o}{2kT_A})], \qquad (14)$$

where $\delta V = V_{max} - V_{min}$ and

$$L \equiv \ln(t/\tau_o) \qquad (15)$$

with the characteristic temperature $T_t = V_{min}/kL$. The logarithm in Eq. (15) can be as large as 30.

Using Eq. (14) one can calculate the temperature T_A^{opt} at which $<\Delta m>$ reaches it peak value. The analytical equations may be expressed for the extremal cases:

$$T_A^{opt} = \begin{cases} 1/2(T_A + T_t) & \text{at } T_A^i \ll \Delta_o/k \\ (T_A T_t)^{1/2} & \text{at } T_A^i \gg \Delta_o/k \end{cases} \qquad (16)$$

Матеріал, захищений авторським правом

Note that the temperature T_A^{opt} is independent of Δ_o only in the limiting cases of Eq. (16), but a dependence $T_A^{opt}(\Delta_o)$ exists also when $T_A^i \sim \Delta_o$.

Thus in an ensemble of randomly distributed two-well potentials, the relative change in occupancy depends on temperature in a nonmonotomic way (when T_A is changed according to the alogrithm previously described) and has a maximum at the temperature $T_A = T_A^{opt}$. The physical cause of this maximum is obvious. At sufficiently high T_A nearly all potentials have fast relaxation times and come to equilibrium in the time t. In equilibrium the mean occupancy of the lower well $\overline{m}$ decreases as the temperature is increased. This is just the behavior of $\Delta\overline{m}(T_A)$ at $T_A > T_A^{opt}$. At a low T_A that is reached by fast cooling from T_A^i the occupancy of the lower well increases as T_A grows, because the 'frozen system' melts during the time t faster at higher T_A. Fig. 9 illustrates these conclusions.

Our interpretation of the experimented data shown in Figs. 4, 6 and 7, is based on the assumption that the measured characteristics are monotonic functions of $<\Delta m>$. Therefore the dependencies $\sigma(T_A)$, $\varepsilon_o(T_A)$, and $\alpha_{1,2}(T_A)$ follow the temperature dependence $<\Delta m(T_A)>$, shown in Fig. 9. This argument is supported by the coincidence of the positions of the maxima in all three curves of Figs. 4, 6 and 7.

It is natural to suppose that the transitions in two-well potentials (Fig. 8) change some electronic states and consequently lead to changes in conductivity and

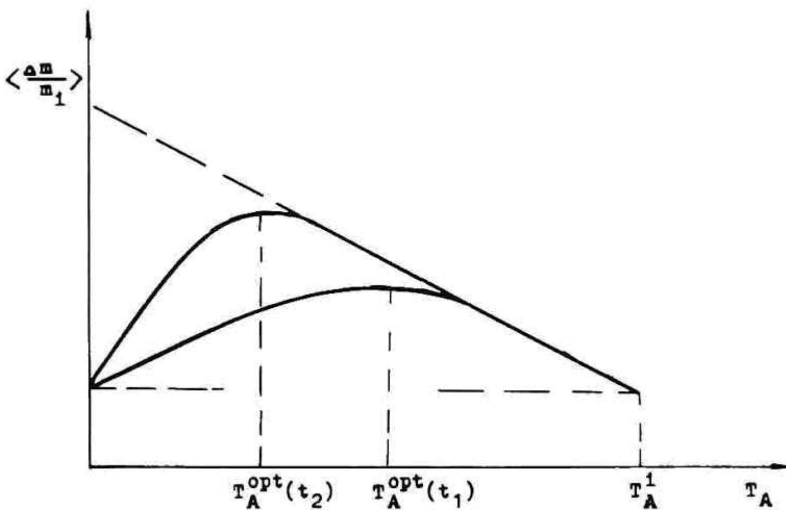

Fig.9 Relative change of lower well occupancy as a function of annealing temperature. Annealing time is t and $t_2 > t_1$.

Матеріал, захищений авторським правом

absorption. Experimental data of other authors[20] testify that the increase in subgap absorption at $h\nu$=1.0–1.2 eV and the increase of the valence band tail slope ε_o correlate with the increase in the spin density of dangling bonds. In our interpretation the growth of $\alpha_{1,2}$ and ε_o is related to an increase of the mean occupancy of the lower wells, as can be seen by comparing Figs. 6 and 7 with Fig. 9. This leads to the conclusion that the lowest energy state is achieved when the defect density reaches a maximum. In other words, we conclude that the ground state of the material is enriched by defects whereas under excitations that lead to transitions to the upper well in Fig. 8 the defect concentration decreases.

Let us extend the previous interpretation to measurements of the temperature dependencies of the conductivity (Figs. 2 and 3). The conduction is considered to proceed via extended states

$$\sigma = \sigma_o \exp(-\frac{\mu}{kT}) \tag{17}$$

where μ is the distance between the Fermi level and the mobility edge. A non-trivial temperature dependence $\sigma(T)$ should be related to a temperature dependence of the Fermi level, μ, which is caused by a variation of the defect concentration $\Delta M = M(\Delta m)$ due to transition in the system of double well potentials (Fig. 8). Assuming that each defect traps only one carrier (an electron or a hole) the shift of the Fermi level through a density of states $g(\varepsilon)$ can be evaluated as:

$$|\Delta\mu| = M\frac{|<\Delta m>|}{g(\mu)}. \tag{18}$$

We suppose that μ gains its maximum value μ_o when the occupancies of the lower wells are equal to unity. Under excitation the transitions from lower to upper wells lead to a decreasing of μ and at $T\rightarrow\infty$, $<\Delta m>\rightarrow 1/2$ and $\mu\rightarrow\mu_\infty$.

We now calculate the temperature dependence of the occupancy m of a single two-well potential upon cooling and heating with constant and finite speed $\xi = dT/dt$. This dependence is determined by the relation between ξ and ξ_T where:

$$\xi_T = (T/\tau_o)\exp(-V/T) \tag{19}$$

For $\xi \gg \xi_T$, the average occupancy $<m>$ cannot follow the temperature variation. Hence it can be regarded as frozen. In the opposite case, when $\xi \ll \xi_T$, $<m>$ follows the temperature variation adiabatically. The value ξ and ξ_T are comparable only in a narrow temperature range of magnitude

Матеріал, захищений авторським правом

$$\Delta T_V = T_V / L \ll T_V \quad \text{where } L = \ln(T_V / \xi \tau_o) \text{ and } T_V = V/kL. \tag{20}$$

T_V is the temperature of equality $\xi = \xi_T$. Fig. 10 presents qualitatively the temperature dependence of $<m>$.

We now discuss the behavior of the conductivity behavior as the temperature is raised from $T=0$, where the sample was considered to be in equilibrium. There are no well-to-well transitions at very low temperatures because of the presence of the minimum barrier $V_{\min}$ in the double-wells. In this case the well occupancies remain unchanged and the Fermi level remains fixed at $\mu = \mu_o$, which corresponds to I of Fig. 11. When the temperature approaches $T_{V_{\min}}$ the frozen-in system of double-wells melts and $<m>$ and μ decrease. The width of the corresponding region II in Fig. 11 is approximately $\Delta T_{V_{\min}}$. As the temperature rises in this region, $<\Delta m>$ rises sharply from zero to approximately $L\,\Delta T_{V_{\min}}/\delta V = V_{\mathrm{mim}}/L\,\delta V$ multiplied by the equilibrium value of $\bar{m}$, corresponding $T = T_{V\min} = T_t$. During subsequent heating $<m>$ can be expressed by using $m(T)$ shown in Fig. 10. Hence

$$<\Delta m> = [\bar{m}(T_1) - \bar{m}(T_2)] \times \begin{cases} \dfrac{LkT_2 - V_{\min}}{\delta V} & \text{for } T_2 < \dfrac{V_{\max}}{kL}, \\ 1 & \text{for } T_2 > \dfrac{V_{\max}}{kL}. \end{cases} \tag{21a}$$

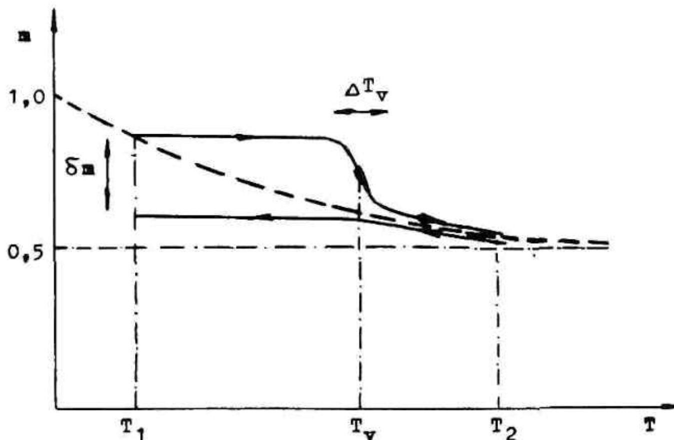

Fig.10 Temperature dependence of lower well occupancy (m) while heating from T_1 to T_2 and cooling at finite rates. Dashed curve shows equilibrium occupancy, δm is hysteresis.

Матеріал, захищений авторським правом

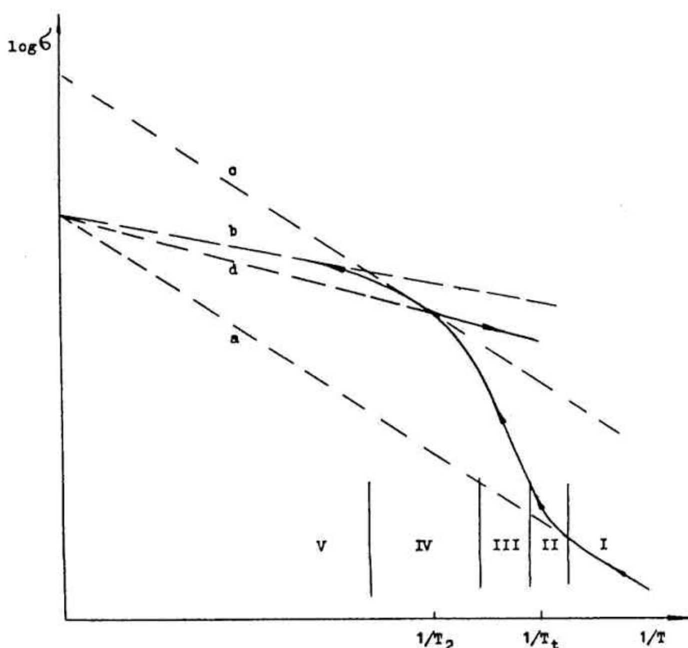

Fig.11 Speculative shape of temperature dependence of conductivity dependence. Dashed curves are related to following activation energies: a - μ_o, b - μ_∞, c - activation energy decreases linearly from μ_o, d- intermediate between μ_o and μ_∞. Regions I-IV are described in the text.

The first factor in Eq. (21a) describes the change of the mean equilibrium occupancy and the second factor is the fraction of double-wells which are in thermal equilibrium at temperature T_2. If the difference between T_2 and T_1 is small, i.e., $T_2 - T_1 \ll T_2$, then Eq. (21a) gives

$$<\Delta m> = \frac{Lk^2}{\Delta_o \delta V}[\ln\cosh(\frac{\Delta_o}{2kT_2}) - \frac{\Delta_o}{2kT_2}\tanh(\frac{\Delta_o}{2kT_2})](T_2 - T_1)\begin{cases} T_2 - T_t & \text{for } T_2 < \frac{V_{\max}}{kL} \\ \frac{\delta V}{kL} & \text{for } T_2 > \frac{V_{\max}}{kL} \end{cases} \quad (21b)$$

The dependence of $<\Delta m>$ on T_2 is close to quadratic when

$$T_2 < V_{\max}/kL \text{ or } T_2 < \Delta_o/k \quad (22)$$

The first inequality implies a linear growth with T_2 of the fraction of potentials that are in thermal equilibrium. The second inequality means that the mean equilibrium occupancies of double-wells depend linearly on T_2. Under these conditions a superlinear change in Fermi level position leads to a temperature dependence of the conductivity as shown by region III in Fig. 11. As the temperature is further

Матеріал, захищений авторським правом

increased, one of the inequalities (22) ceases to hold and consequently $<\Delta m>$ approaches a linear T dependence. This is reflected by region IV in Fig. 11. A further growth of T_2 disturbs both inequalities (22). The Fermi level approaches then its extreme position μ_∞ and practically becomes independent of temperature. It should also be emphasized that the values of the conductivity activation energy in regions II and III have no physical meaning and may be greater than E_g.

Now we analyze the $\sigma(T)$ dependence during cooling as the temperature decreases from T_2 to $T_1<T_2$. This T-dependence is not the same as that observed during heating. There is some hysteresis caused by frozen-in potentials which practically do not change their occupancies. Fig. 10 shows that the contribution of double-wells with fixed $T_V=V/kL$ is equal to $\delta m=\overline{m}(T_1)-\overline{m}(T_V)$. Hence, the resulting hysteresis can be obtained by averaging δm over all barriers:

$$<\delta m> = \int_T^{T'} \left(\frac{kT}{\Delta_o}\ln\cosh\frac{\Delta_o}{2kT} - \frac{kT_V}{\Delta_o}\ln\cosh\frac{\Delta_o}{2kT_V}\right)\frac{LkdT_V}{\delta V} \tag{23}$$

where $T=\max(T_1,T_t)$, $T'=\min(T_2, V_{max}/kL)$ and $T<T'$. We mention as an example that at $T_2-T_1 \ll T_2$ the hysteresis is

$$<\delta m> = \frac{Lk^2}{2\Delta_o \delta V}[\ln\cosh(\frac{\Delta_o}{2kT_2}) - \frac{\Delta_o}{2kT_2}\tanh(\Delta_o/2kT_2)](T_2-T_1)^2 \tag{24}$$

Comparing this with Eq. (21b) one finds that at $T=T_t$ the hysteresis is about one half of the $<\Delta m>$ change during heating. But in general the value of $<\delta m>/<\Delta m>$ is larger than 0.5. When the hysteresis is well pronounced, the Fermi level is practically immobile during cooling. The corresponding conductivity change is shown in Fig. 11. We believe that the temperature dependence of the conductivity shown in Fig. 11 presents a phenomenological explanation of the experimental data shown in Fig. 2. A comparison of the curves of Fig. 2 and 11 enables us to estimate the parameters of our phenomonological model.

The temperature dependence of the conductivity in another possible measurement regime is shown in Fig. 12. At the beginning, the sample is swiftly cooled down to temperature T_2. After resting at this temperature for a long time, it is then rapidly heated. Just this regime was realized by Street et al.[1] The details of the conductivity curve are found to depend on the prior history of sample. Thus the $\sigma(T)$ dependence would be flat if the Fermi level does not sink below the equili-

Матеріал, захищений авторським правом

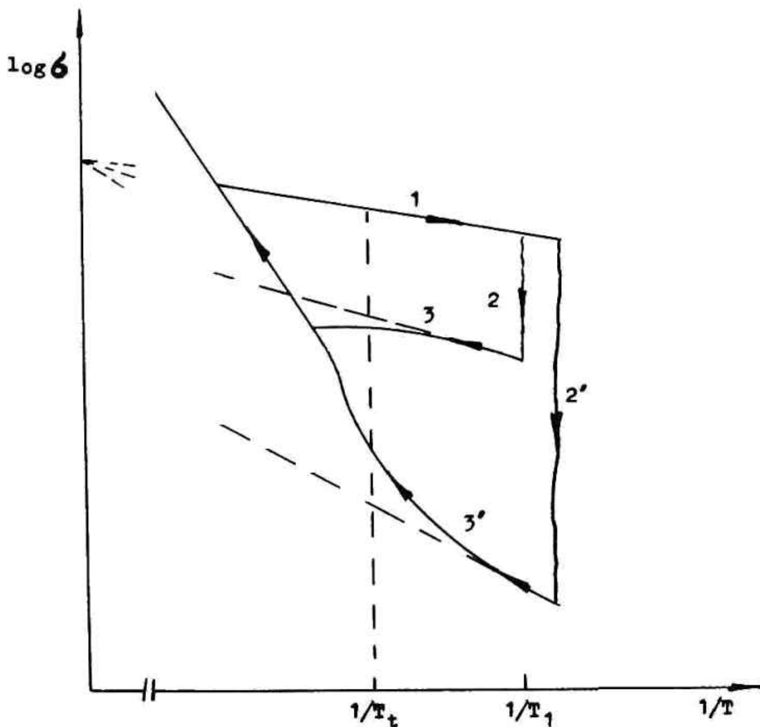

Fig.12 Temperature dependencies of conductivity with are predicted in the following regions:
1 - fast cooling, 2 insothermal annealing at T_1, 3 - fast heating. The period of isothermal annealing in 1, 2, 3 processes is less than in 1, 2′, 3′ processes.

brium value $\mu(T_t)$. In the opposite case when the time of rest is sufficiently long to permit the Fermi level to descend below $\mu(T_t)$, the $\sigma(T)$ dependence is much steeper because the Fermi level moves quickly with increasing temperature. Similar dependencies have been observed by Street et al.[1] in doped material and by us in the present work on undoped material. The activation energy was found to increase with the resting time in agreement with our theoretical predictions which are schematically shown in Fig. 12. Here curves 1, 2 and 3 are converted into curves 1, 2 and 3, respectively, as the resting time t is increased.

Consider now the time relaxation of the frozen-in conductivity. Let the temperature drop sharply from T_2 to $T_1 > T_t$. In this case the conductivity remains frozen-in, following curve d in Fig. 11. Its relaxation law is defined by a shift of the Fermi level to the equilibrium position $\mu(T_1)$, i.e.:

Матеріал, захищений авторським правом

$$\sigma \propto \exp\{-\frac{\Delta\mu(t)}{kT}\} = \exp\{-\frac{M<\Delta m(t)>}{g(\mu)kT}\} \tag{25}$$

Taking $<\Delta m(t)>$ from Eq. (14) one finds

$$\sigma \propto (\frac{t}{\tau_{\min}})^{-\gamma} \text{ and } \tau_{\min} = \tau_o \exp(\frac{V_{\min}}{kT_1}) \tag{26}$$

where

$$\gamma = \frac{Mk}{g(\mu)\Delta_o \delta V}[T_1 \ln\cosh(\frac{\Delta_o}{2kT_1}) - T_2 \ln\cosh(\frac{\Delta_o}{2kT_2})]. \tag{27}$$

Thus the relaxation of the frozen-in conductivity follows a power law. This prediction is in a good agreement with the experimental results of Street et al.[1] and with the results obtained in the present work (see Fig. 3).

The model under discussion allows us to compare the results of temperature cycling with those of frozen-in conductivity measurements. Eqs. (14), (18) and (27) enable us to find a relation between $\gamma \approx 0.4$–0.5 and the relative change of the conductivity at temperature $T_A^{\rm opt}$ in Fig. 4. It should be emphasized that T_A^{opt} is here the annealing temperature, and all measurements after T-cycling were carried out at room temperature. The relation is

$$\ln[\frac{\sigma_{\rm room}(T_A^i)}{\sigma_{\rm room}(T_A^{\rm opt})}] = \gamma L\,(T_A^{\rm opt} - T_t)/T_A^{\rm room} \tag{28}$$

The right hand side of Eq. (29) is equal to 2.4 if we assume that in accordance with previous results $T_A^{\rm opt} - T_t = 60$K, $T_A^{\rm room} = 300$K, $\gamma = 0.4$ and $L = 30$ is the most reasonable value. This value 2.4 is in good agreement with the value of the logarithm in (28), which is equal to 1.8. Considering the uncertainty in the $T_A^{\rm opt}$ and γ measurements as well as the somewhat arbitrary choice of L (with a possible error of about 10%), we can conclude that Eq. (28) is supported by experiment.

We now evaluate the parameters of our model. The lower temperature kink of the $\sigma(T)$ curve in Fig. 2 is situated at $T \approx 0^o C$, which yields $T_t \approx 0^o C$. This value leads to $V_{\min} \approx 0.7$ eV for $L = 30$. With this T_t value and $T_A = 200^o C$ we obtain from Eq. (16) $T_A^{\rm opt} \approx 100^o C$ when $T_A^i \ll \Delta_o / k$ and $T_A^{\rm opt} \approx 90^o C$ when $T_A^i \gg \Delta_o / k$. These values agree well with the experimental value $T_A^{\rm opt} = 60^o C$. It should be noted that the proximity of the $T_A^{\rm opt}$ values estimated for the two extreme cases implies that $\Delta_o \sim kT_A^i$. Hence Δ_o may be estimated to be 0.04 eV. This value should be substi-

Матеріал, захищений авторським правом

tuted into Eq. (27). Assuming T_1=20°C, T_2=200°C, γ=0.4 one obtains $M/g\,\delta V$=0.5. Let us now analyze the Eqs. (21b) and (18). They predict a linear shift of the Fermi level with temperature above the high temperature kink position in Fig. 2 or in region IV of Fig. 11. A linear shift βT of the Fermi level results in an increase of the preexponential factor σ_o by $\exp(\beta/k)$ relative to its value at $T \leq T_t$. The measured value $\Delta\log\sigma_o \approx 2$–3 (Fig. 2) should be compared with Eq. (21b) assuming $T_2 < V_{max}/kL$. In the following we show that V_{max} is approximately equal to the hydrogen diffusion activation energy, i.e., $V_{max} \approx 1.5$ eV.[14] In summary, the parameters of our model have the following values: $\Delta_o \approx 0.04$ eV, $V_{min} \approx 0.7$ eV, $V_{max} \approx 1.5$ eV, $M/g(M) \approx 0.4$ eV.

Our model allows us therefore to explain in a consistent way all experimental results concerning metastable thermal processes. We believe that the results obtained by Street et al.[1–5] can be explained by the same model although the numerical parameters may differ from ours.

We now turn to our assumption that the lower minimum of the double-well potential is related to the defect rich configuration of a–Si:H. This assumption contains two uncertainties. First, it implies that under any external action the defect concentration cannot change more than by a factor of two, namely from 1/2 to 1. Second, it is quite unclear why in amorphous systems which have considerable structure defects, the difference ΔE in energy between defect poor and defect rich configurations is always positive while it can be very close to zero. We suggest two explanations. The first is the following: One should admit the presence of configurations with a different sign of ΔE. Simultaneously it should be supposed that the concentration of configurations with $\Delta E > 0$ is higher and hence plays the dominant role. This supposition explains the above uncertainties. Another explanation will be developed in the next section. Its main idea is that the applicability of our phenomenological approach is quite limited and in reality metastable thermal processes cannot be fully described by the simplest form of the double-well potential model.

5. FLUCTUATIONS IN DISORDERED SYSTEMS

In this section we discuss the general problem of the interation between electrons and mobile impurities in disordered systems. In the next chapter we concretize the general model for a–Si:H where the role of impurity is played by hydrogen.

Материал, защищенный авторским правом

Let us analyze the reduction in total energy due to a rearrangement of bonded hydrogen atoms via an interaction with localized electrons. The idea, that in the presence of localized carriers neutral impurities can form spatial configurations leading to a decrease in total energy, was proposed by Krivoglaz[21] for crystalline materials. Self-bound states of neutral impurities and localized electrons were called fluctuons by him. We consider here similar states in a–Si:H with hydrogen playing the role of neutral impurities. Following Krivoglaz we call these formations fluctuons even though they are quite different from fluctuons in crystals.

The main features of Krivoglaz' theory are the following. The kinetic energy of an electron localized in an area with linear dimensions R is of order $\hbar^2/mR^2$ while its potential energy depends linearly on the local impurity concentration n. The deviation Δn from its average value may lead to a reduction in electron energy by $A'\Delta n$, where A' = const. But it leads to a decrease of entropy and an increase in free energy approximately by the value $TR^3\Delta n$. As a consequence, the free energy can be expressed as:

$$F \approx -A'\Delta n + \frac{\hbar^2}{mR^2} + TR^3\Delta n \tag{29}$$

without taking account interactions between impurities. At any given value F reaches a minimum at $\Delta n = 0$ or Δn_{max}, when the impurity either occupies or leaves all available sites in the neighborhood of the localized electron. In fact, Δn should be fixed at $\Delta n_{max} \sim a^{-3}$, where a is the characteristic interatomic distance. Then to minimize Eq. (29), R should be approximately equal to $(\hbar^2/mT\Delta n)^{1/5} \gg a$. Hence the fluctuon is spread over many elementary crystalline cells. This approach is characterized by the appearance of an impurity phase.

The greatest difference between crystalline and amorphous solids is that the potential relief of impurity atoms in an amorphous system is randomly disturbed due to the disorder. An example of such a distribution is shown in Fig. 13. To simplify our considerations we suppose that the energetical minima are randomly distributed in range B. At $T=0$ the potential wells consequently are filled by impurity atoms from a minimum energy up to a certain demarcation energy μ_i (Fig. 13).

Consider now a sphere of radius $R > a$, where the electron is localized at energy E_o below the mobility edge. As in Eq. (29) the electron interacts linearly with the local impurity concentration. But unlike in crystals the deviation of the

Матеріал, захищений авторським правом

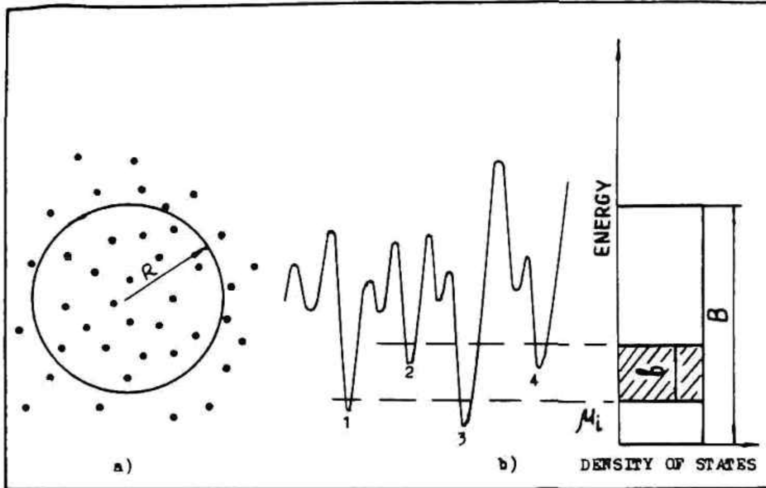

Fig.13 (a) A fluctuation of hydrogen concentration in the region of electron localization at fluctuon formation;

(b) Random potential relief for hydrogen atom and energy distribution of potential minima. Minima 1 and 3 are filled in the absence of electron. In the presence of electron minima 2 and 4 are filled too. This is the fluctuon formation.

local concentration from its mean value leads to an energy loss even at zero temperature. Specifically, suppose that ΔN extra impurities are introduced in a localization region containing $(R/a)^3$ sites. They fill energetical minima in a range from μ_i to μ_i+b, where $b=B(a/R)^3\Delta N$ (see Fig. 13). Hence the energy increase is $(1/2)b\,\Delta N=(B/2)(a/R)^3(\Delta N)^2$ and the total energy of the fluctuon is

$$E = E_o - A\left(\frac{a}{R}\right)^3\Delta N + \frac{B}{2}\left(\frac{a}{R}\right)^3(\Delta N)^2 \tag{30}$$

It reaches a minimum value when

$$\Delta N = N_o \equiv \frac{A}{B} \tag{31}$$

Then

$$E = E_o - W_o \quad \text{where } W_o = \frac{A^2}{2B}\left(\frac{a}{R}\right)^3 \tag{32}$$

Here and later we assume for clarity that $A>0$, which corresponds to an energy decrease when the impurity concentration increases in the localization volume. Also for simplicity we consider fluctuon formation around a localized electron only because the effects are qualitatively the same for holes.

Матеріал, захищений авторським правом

Expressions (30) - (32) are formally the same as those for polarons, when deformation is substituted by excess concentration of impurities, and W_o in Eq. (32) is playing the role of the polaron shift.

We do not consider the detailed shape of the localized electron wavefunction. In the present model the wavefunction is characterized by the localization radius R only. In principle, the magnitude of R can be estimated self-consistently by satisfying the minimum $E(R)$ with $E_o(R)$ given. But in a real amorphous system the function $E_o(R)$ is not known. That is why we use $R \sim 10$Å as an empirical estimate of the localization radius in a–Si:H.[22]

The parameter A can be estimated in the following way. In the hypothetical case when $R=a$, the energy of interaction between the electron and the impurity will be of the same order as in an atom, i.e., $A \sim 10$ eV. The parameter B, that characterizes the potential fluctuations, can be estimated from experimental data about impurity diffusion rates in amorphous alloys,[23] which give $B \sim 1$ eV. Assuming $R/a \sim 10$, one obtains the values $N_o \sim 10$ and $W_o \sim 0.1$ eV. The short-order interaction between impurities can be neglected because $N_o \ll (R/a)^3$. It also follows that $b \ll B$.

Eqs. (30) - (32) define only average values of the parameters. There are fluctuations in these values which are produced by variations in the impurity potential wells in the neighborhood of the localized electron. To investigate such fluctuations let us consider a layer of width b above the Fermi level μ_i (Fig. 13). When ΔN excess impurities are introduced in this energy layer in the neighborhood of the electron, the absolute variation in energy is

$$W = A\left(\frac{a}{R}\right)^3 \Delta N - \frac{1}{2} b\, \Delta N \tag{33}$$

Fluctuations are caused by deviations of ΔN from its mean value.

$$\Delta \bar{N} = \frac{b}{B}\left(\frac{R}{a}\right)^3 \tag{34}$$

The distribution of fluctuations under consideration obeys Poisson's law

$$\frac{(\Delta \bar{N})^{\Delta N}}{(\Delta N)!} e^{-\Delta \bar{N}} \equiv \exp\{-S(\Delta N, \Delta \bar{N})\} \tag{35}$$

Материал, защищенный авторским правом

Optimization of the exponent in Eq. (35) permits us to express the probability distribution of fluctuonic energies as

$$\rho(W) \propto \exp\{-S_o(W)\}, \tag{36}$$

where

$$S_o(W) = \left(\frac{W-W_o}{W_o}\right)^2 N_o \ \text{for}\ |W-W_o| \ll W_o, \tag{37}$$

$$S_o(W) = \frac{WN_o}{W_o}\ln\left(\frac{W}{W_o}\sqrt{N_o}\right) \ \text{for}\ W \gg W_o.$$

It is clear that the probability for fluctuations decreases strongly as W increases. In the following we ignore this W dispersion altogether and assume $W=W_o$. This simplification does not influence our general results. A more detailed analysis of the effect of W dispersion has been carried out by Karpov et al.[12]

Let us now discuss fluctuons at finite temperatures. We introduce a new term related to entropy in the expression for the free energy

$$F = E_o - W_o + \frac{W_o}{N_o^2}(N - N_o - \bar{N})^2 + kT\ln\frac{N}{\bar{N}}. \tag{38}$$

The first three terms give the mean energy of the fluctuon, Eq. (30), having N impurity atoms in the localization region. Minimization of Eq. (38) leads to

$$Z + \ln Z = \Theta,$$
$$Z \equiv \frac{N}{N_o}\,\frac{T_f}{T}, \tag{39}$$
$$\Theta \equiv T_f T + \frac{T_f}{T}\,\frac{\bar{N}}{N_o} + \ln\left(\frac{T_f}{T}\,\frac{\bar{N}}{N_o}\right),$$

where

$$T_f = \frac{2W_o}{kN_o} \tag{40}$$

T_f plays the role of the characteristic temperature of fluctuon disintegration due to 'evaporation' of impurity atoms. For low and high temperatures Eq. (40) gives

Материал, защищенный авторским правом

$$N = (N_o+\bar{N})\{1-\frac{T}{T_f}\frac{N_o}{N_o+\bar{N}}\ln(1+\frac{N_o}{\bar{N}})\} \text{ for } T \ll T_f, \tag{41}$$

$$N = \bar{N}(1+\frac{T_f}{T}) \text{ for } T \gg T_f.$$

It should be emphasized that Eqs. (38) - (41) are valid when the impurity concentration n is much greater than the electron concentration n_e, that is when $n \gg N_o n_e$. Only under this condition are fluctuons formed and exist independently of each other. In the opposite case, when $n \leq N_o n_e$ the behavior of the system is quite different. We will not discuss this situation here because in a–Si:H, the hydrogen concentration $n \sim 10^{21}\text{cm}^{-3}$ is much higher than the concentration of localized electrons $n_e \sim 10^{19}\text{cm}^{-3}$ even when $N_o \sim 10$.

We shall now finish the general description of the fluctuon model and discuss its consequences for a–Si:H in order to understand the metastable thermal processes described earlier in section 4.

6. FLUCTUON MODEL OF a–Si:H

In this chapter we apply the fluctuon model to a–Si:H. Here the role of moving impurity atoms is played by hydrogen atoms. Hydrogen diffusion is appreciable between 300 and 500K and may change spatial configurations during the time of the experiment. The general result of the previous chapter, which we use here, is that fluctuon formation reduces the energy by a value W equal to several tenth of electron volt and that fluctuons disintegrate at a characteristic temperature T_f which is of the order of several hundred degrees Kelvin.

We suppose that fluctuons are formed with assistance of electrons that are localized on defects such as dangling bonds, which are the dominant defects in the mobility gap. It is known that the hydrogen concentration in a–Si:H substantially exceeds that of dangling bonds. Hydrogen leads to passivation of dangling bonds by the formation of stronger Si:H bonds having more compact wave functions. This means that passivated bonds are less sensitive to the surrounding local configurations of hydrogen atoms. In other words, the fluctuonic effect is suppressed by the dangling bond passivation.

Матеріал, захищений авторським правом

At a given temperature there is equilibrium between the concentrations of passivated and non-passivated dangling bonds. Upon heating this equilibrium is shifted towards passivated bonds. The decrease in non-passivated dangling bond concentration is caused by thermally induced disintegration of fluctuons. The increase in fluctuon energy makes passivated bonds preferable. This mechanism is illustrated in Fig. 14.

This situation can be explained from another point of view. Let us divide the hydrogen atoms into two groups: 'passivating' hydrogen atoms (H_p) and 'non-passivating' hydrogen atoms (H_{np}). We use here the term 'passivating hydrogen' for those atoms which would originate dangling if they were removed. 'Non-passivating hydrogen' is clustered hydrogen and weakly bonded hydrogen for example, in other words, all hydrogen which does not produce dangling bonds when it is removed. The energy distributions of these two kinds of hydrogen are shown in Fig. 15. The origins of the H_p and H_{np} distributions are energy fluctuations in amorphous systems such as a–Si:H. The shapes of the distributions sketched in Fig. 15 are determined from the following well known facts: (i) The H_p concentration is a small fraction of the total hydrogen concentration, (ii) the largest fraction of dangling bonds is passivated, (iii) the total hydrogen concentration in a–Si:H is much larger than that needed to passivate dangling bonds. Fluctuons are mostly formed with the assistance of H_{np} atoms. Thermal decomposition of fluctuons forces hydrogen atoms to leave fluctuons and to increase their energy. This process can be represented by a shift of the H_{np} distribution in Fig. 15 to higher energies, hence the H_p concentration increases. In other words passivation grows with temperature.

The above speculations mean that there are two kinds of neighboring energy states: fluctuonic states which include dangling bonds and the states of bonds passivated by hydrogen. These two kinds of states correspond to substantially different local configurations of hydrogen which are schematically shown in Fig. 14 and 16. The transition of an electron between these two states is followed by hydrogen diffusion. In a–Si:H the magnitudes of the potential barriers for diffusion fluctuate in some range $V_{min}<V<V_{max}$, where V is approximately 1 eV. This value is much larger than the energy barrier $W/4$ between the two wells shown in Fig. 16.

Матеріал, захищений авторським правом

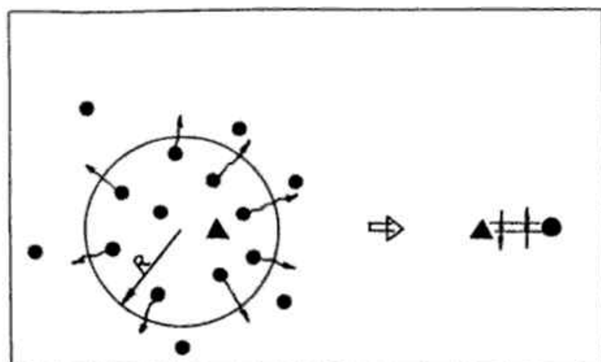

Fig.14 Dangling bond passivation upon heating. Left side shows fluctuon disintegration which occurs by hydrogen 'evaporation'. Triangle is three-fold coordinated atom of silicon with one dangling bond. The radius of electron localization on dangling bond is R. Fluctuon disintegration increases energy of system hence passivation is energetically favorable. Black circles are hydrogen atoms.

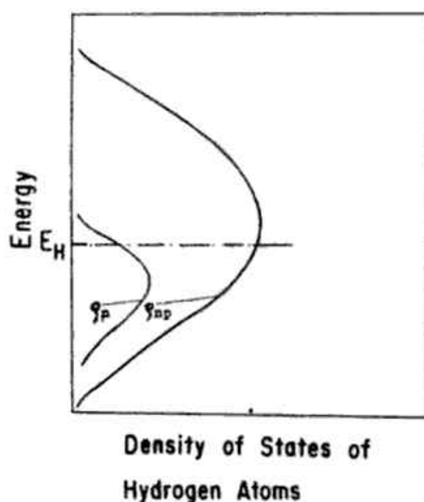

Fig.15 Passivating, $\rho_p(E)$, and non-passivating, $\rho_{np}(E)$, distribution of hydrogen. The states situated higher that E_H are empty, those lower than E_H are filled. Total hydrogen concentration is $\int_0^{\infty}[\rho_p+\rho_{np}]dE$. Relatively small concentration of unpassivated dangling bonds is $\int_{E_H}^{\infty}\rho_p(E)dE$.

Материал, защищенный авторским правом

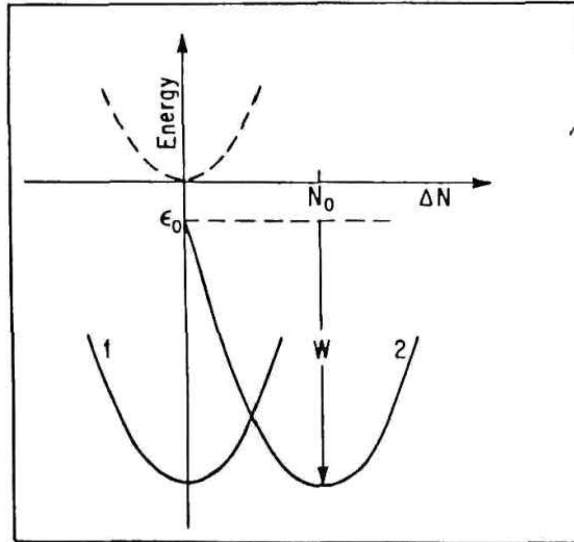

Fig.16 Passivated bond (1) and fluctuon (2) energies as a function of number of excess hydrogen atoms in the region of electron localization. Dashed line shows the energy of excess hydrogen atoms expressed by Eq. (42). ε_o is initial energy of an electron in the absence of hydrogen atoms, W is energy shift due to fluctuon formation.

Hence the transition rate between the two wells is determined by the heights of the diffusion barriers. It should be mentioned also that the energies of the left and of the right minima are distributed because of fluctuations in the values of E_o and W and fluctuations of passivated bond energies. Hence there exists occasional asymmetries ΔE between two minima in Fig. 16. The sign of ΔB can be negative or positive. To this extent the present model agrees with the phenomenological model of double-well potentials given in Chapter 4 and provides its physical interpretation.

However, this agreement has its limitations. We assumeed that the parameters of the double-well potential of Fig. 8 are independent of temperature. This very common assumption is not made in the fluctuon model. At finite temperatures one should analyze free energies $F = E + kTN\ln(N/\overline{N})$, instead of energies of two states. The functions $F(N)$ does depend on temperature in contrast to $E(N)$ in Fig. 16. The difference between the energies of the minima grows with temperature:

$$\Delta E = \text{const} + N_o kT\ln(N/\overline{N}) \tag{42}$$

Матеріал, захищений авторським правом

Consequently, the double-well potential asymmetry depends on temperature and the energy of defect rich state grows as the temperature increases regardless of the sign of ΔE. Taking into account the temperature dependence of the number of hydrogen atoms in fluctuons defined by Eq. (41) one can easily see that ΔE depends strongly on temperature at $T \leq T_f$. At $T > T_f$ one finds $N \approx \overline{N}$, and the temperature dependence of Eq. (42) vanishes. So the concentration of fluctuon defect states decreases while the concentration of passivated bonds grow as the temperature increases for $T \leq T_f$ because of the temperature dependence of ΔE in the phenomenological double-well potential model in Chapter 4. Now it can be introduced incorporated in the phenomenological model by using the limit $\Delta_o = kT$ for the width of the distribution of occasional energies ΔE. In this way the occupancies of the wells vary with temperature only for $T \leq T_f$, in agreement with the fluctuon model. Hence, the magnitude of Δ_o estimated in Chapter 4 yield a value for T_f of $T_f \approx \Delta_o / k = 400$K. This value agrees well with the theoretical estimate of T_f obtained in Chapter 5.

Another remark about the accord between the phenomenological model and the fluctuon model concerns the kinetic properties. The fluctuon model suggests that transitions between two states are related to hydrogen diffusion in the random potential relief. The properties of such diffusion are determined by the topology of the available ways for random walks. Preliminary analysis shows that these ways form a fractal with a dimension that depends on temperature. The problem requires additional discussions that go beyond the scope of this article. We wish to remark only that at the initial stage the relaxation is governed by unique hops of atoms while substantial transitions are not important. Hence the phenomenological model seems to give an essentially identical description of the relaxation at its initial stage.

7. CONCLUSIONS

In summary we wish to emphasize the following results.

1. We carried out new experiments in which electrical and optical parameters of a–Si:H were measured in response to cyclically varying temperature. The quantities we measured depend non-monotonically on the annealing temperature T_A. The shapes of these dependencies and particularly the positions of the maxima yield information about processes in the disordered system. Here we present the results of cyclical measurements of the conductivity, the absorption coefficient and the slope of Urbach tail. In future we plan to carry out similar measurements of the photoconductivity and photoluminescence in intrinsic and doped samples.

Матеріал, захищений авторським правом

8. A.A. Andreev, T.A. Sidorova, E.A. Kazakova, M.S. Ablova, A. Ya. Vinogradov, Fiz. Tech. Poluprov. 20, 1469 (1986); Sov. Phys. Semicond. 20, 1469 (1986).
9. ZE. Smith and S. Wagner, Phys. Rev. Lett. 59, 688 (1987).
10. K. Shepard, ZE. Smith, S. Aljishi and S. Wagner, Appl. Phys. Lett 35, 1644 (1988).
11. T.J. McMahon and R. Tsu, Appl. Phys. Lett. 51, 412 (1987).
12. V.G. Karpov. V.N. Solovijev, Fiz. Tverdogo Tela, 31, 5 (1989); Sov. Phys. Solid. State, 31, 5 (1989).
13. T. Tiedje, 1984, in "The Physics of Hydrogenated Amorphous Silicon II", edited by J.D. Joannopoulos and G. Lucovsky (Springer-Verlag, Berlin, 1984) p
14. R.A. Street, C.C. Tsai, J. Kakalios and W.B. Jackson, Philos. Mag. B 56, 305, (1987).
15. M. Vanecec, J. Kocka, J. Stuchlik, Z. Kozisek, O. Stika, A. Triska, Sol. Energy Mater. 8, 411 (1983).
16. P.W. Anderson, B.I. Halperin and C.M. Verma, Philos. Mag. 25, 1 (1975).
17. "Amorphous Solids: Low Temperature Properties", ed. by W.A. Phillips (Springer-Verlag, Berlin, 1981).
18. M. Stutzmann, W.B. Jackson and C.C. Tsai, Phys. Rev. B 32, 23 (1985).
19. D. Redfield, J. Non-Cryst. Solids 97/98, 783 (1987).
20. L. Ley, 1984, in "The Physics of Hydrogenated Amorphous Silicon II", edited byJ.D. Joannopoulos and G. Lucovsky (Springer-Verlag, Berlin, 1984) p
21. M.A. Krivoglaz, Uspehi Fiz. Nauk, 111, 617 (1973) (in Russian).
22. R.A. Street, Adv. in Phys. 30, 593 (1981).
23. V.N. Solovijev, Phys. Stat. Solidi (a) 83, 553 (1984).
24. D.L. Staebler and C.R. Wronski, J. Appl. Phys. 51, 3262 (1980).

Материал, защищенный авторским правом